Wind Changes over the Western Pacific

W. Timothy Liu, Xiaosu Xie, and Wenqing Tang
Jet Propulsion Laboratory, California Institute of Technology, Pasadena, CA 91109

1. Introduction

The history of China has been swayed by winds over the Western Pacific. Winds carried the Eunuch Admiral, Zheng He, and his fleet to the Indian Ocean and Africa in the 15th century, dazzling the maritime countries with the riches and power of the Ming Dynasty. A century later, European traders, following the Portuguese Admiral Vasco da Gama, rode the winds and gave the Ching Empire the ultimate humiliation with extraterritoriality and colonies. Through millennia, steady winds have brought rain to nourish the agrarian economy of the Yangtze and Pearl delta, but the vagaries of wind and rain have also devastated livelihoods and governments. The consequences of ocean winds may be well observed over land, but their breeding grounds over the oceans are not adequately monitored. Observations of marine winds, with adequate spatial and temporal scales to monitor and predict their environmental and climatic effects, can be achieved only from the vantage point of space. A few examples to demonstrate the impact of the most recent spacebased wind observations are given in this brief report.

2. Global Wind

Fig. 1 is based on preliminary data derived from the SeaWinds scatterometer on QuikSCAT of the National Aeronautics and Space Administration (NASA) [Graf et al., 1998]. It was launched in June 1999 to replace the NASA Scatterometer (NSCAT). A scatterometer sends microwave pulses to the Earth's surface and measures the backscatter power from the surface roughness. The roughness may describe characteristics of polar ice or vegetation over land. Over the ocean, which covers more than three-quarters of the Earth's surface, the backscatter is largely due to small (centimeter) waves on the surface. The idea of remote sensing of ocean surface winds was based on the belief that these surface ripples are in equilibrium with the local wind stress. The backscatter power depends not only on the magnitude of the wind stress but also on the wind direction relative to the direction of the radar beam. The capability of measuring both wind speed and direction is the major uniqueness of the scatterometer.

In the figure, the strong (violet color) trade winds blow steadily from the cooler subtropical oceans to the warm water of the Intertropical Convergence Zone (ITCZ) located just north of the equator. The air rises over the warm water of the ITCZ and sinks in the subtropics at the horse latitudes, forming the Hadley Circulation. Both the convergence area at the ITCZ and the divergence area at the horse latitudes are indicated by low wind speed of blue color. In the midlatitudes, the high vorticity caused by the rotation of the Earth generates storms (yellow spirals), particularly in the southern oceans, which are in winter. The eastern North Pacific is dominated by a persistent high-pressure system, whose anticyclonic (clockwise) flow creates strong winds blowing parallel to the coast of Canada and the United States. This creates strong ocean upwelling and a few degrees of cold temperature anomalies along the coasts of the US. Typhoon Paul is observed south of Japan, and tropical depression Rachael is forming southeast

of Taiwan. Tropical depression Eugene is visible as close circulation in the eastern Pacific off Central America.

The ocean is largely covered by clouds, which prevent observations of the sea surface by instruments measuring at infrared and visible frequencies. Because the atmosphere is largely transparent to microwaves, SeaWinds was able to cover 93% of the global oceans, under both clear and cloudy conditions, in a single day. Objective interpolation is used to produced the uniformly gridded map [Tang and Liu, 1996]. Weather satellites, despite their frequent coverage, can view only part of the world's oceans. SeaWinds, on the other hand, provides in Fig. 1 a synoptic view of tropical cyclones in both the eastern and western Pacific. Spaceborne scatterometers have the capability of synoptic global coverage and high spatial information [see also Liu et al., 1998]. Atlas et al. [1999] showed NSCAT winds improve significantly the forecasts and analyses of global numerical weather prediction models. Chang et al. [1998] took advantage of the high spatial information of NSCAT winds to improve regional precipitation forecasts in Taiwan. The normalized backscatter coefficients over land are related to land vegetation, and those over Antarctica provide information of sea-ice extent and morphology [Long and Drinkwater, 1999].

3. Typhoon

The scatterometer was not designed to study tropical cyclones. The relation between radar backscatter and wind vector under strong wind and high precipitation conditions is not well established. Because of the strong economic and environmental impact, however, scatterometer data have been applied in studying and monitoring tropical cyclones. Hsu and Liu [1996] used scatterometer winds to derive pressure field, and thus to improve the estimation of location and intensity of tropical cyclones. NSCAT winds were also used by Liu et al. [1998] to study the extratropical transition of a typhoon.

Fig. 2 shows that Typhoon Olga is fully covered by the 1800-km continuous swath of Quikscat. The 25-km resolution provides good details of surface winds, which feed moisture to fuel the severe storm. Over the ocean, in situ observations in a tropical cyclone are extremely sparse, and conventional satellite data provide only cloud imagy at the top of the storm. Tropical cyclones are devastating when accompanied by strong winds and heavy precipitation. Coincident measurements of wind and precipitation are important in understanding the structure of the storm and to predict its path. QuikSCAT and the Tropical Rain Measuring Mission (TRMM) provide the only opportunity to observe both the dynamic and hydrologic parameters before landfall. The coincident measurements of surface winds and precipitation reveal the interplay between dynamics and the hydrologic balance of the storm. Liu et al. [1999] used data from QuikSCAT to improve the estimation of the precipitation profile in Hurricane Floyd and compared the results with measurements from both the radiometer and radar on TRMM.

4. Flood

Nghiem et al. [1999] demonstrated that the ratio of the vertical to the horizontal backscatter coefficients over flat terrain is related to the extent of flooding. SeaWinds observations coincide

with extensive floods in Asia caused by strong monsoons and tropical cyclones. The maps in Fig. 3 show that the flooding in the Yangtze Valley of China (30°N), represented by blue patches, is clearly visible in July, following strong summer monsoons. The flooding recedes in September, with the retreat of the summer monsoon and the advance of the winter monsoon. The intensity of the flooding increases again in October, after the landfall of a typhoon. The flood in Bangladesh and east India did not start until August but continues to strengthen through October. The most severe floods in Vietnam, Thailand, and Burma occurred in August and September, at the peak of summer monsoons. Scatterometers are capable of monitoring not only the ocean winds, which feed moisture, but the consequent flooding of the land.

5. Monsoon and El Niño

Monsoons are the seasonal change of wind forced by continent-ocean temperature contrast. The oceanic response to the seasonal changes of Asian monsoons was studied by Liu and Xie [1999] using satellite data. A longer time-series of ocean surface winds derived by combining the wind speeds measured by the Special Sensor Microwave Imager (SSMI) and all available wind direction data through variational analysis [Liu et al., 1996] was used to examine the relation between Asian monsoons and the interannual El Niño Southern Oscillation. The winter composites of anomalous cold evens (La Niña) in Fig. 4 show that cold temperature anomalies prevail in the equatorial central to eastern Pacific and warm temperature anomalies occur in the equatorial western Pacific, extending to high latitudes in the central Pacific. Associated with the temperature pattern, anomalous easterly winds dominate the equatorial central Pacific and an anomalous cyclonic gyre center in the Philippines. The cyclonic anomalies appears to cause lower sea level and sea surface temperature (SST) in the marginal seas of the western Pacific, most likely due to increased upwelling in the ocean, which in turn may reduce the zonal temperature and thermocline gradient in the western Pacific, providing a negative feedback to the La Niña event. The northeast anomalies over the South China Sea during winter mean a stronger than normal monsoon. The abundant moisture is brought into the basin by the intensified northeasterly winds from the Philippine Sea and East China Sea where SST is abnormally warm, leading to a high moisture supply in the basin, and less than normal latent heat flux, despite strong winds. The cooler SST is caused by ocean dynamics and not by local surface cooling

6. Data

SeaWinds data in standard formats for scientific application are distributed by the Physical Oceanography Distributed Active Archive Center at the Jet Propulsion Laboratory (JPL) in a delayed model (weeks after observations). A number of scientists are planning to produce high-level interpolated wind fields from these data. Near-real time (a few hours after observations) data will be distributed by the National Oceanic and Atmospheric Administration (NOAA) to operational weather forecast agencies. A data system, Seaflux, has been established, the initial phases of which are to produce, display, and disseminate high-level (uniformly gridded) SeaWinds data, including wind vector, stress, and their derivatives, in near-real time, every 12 hours. The surface winds are also combined with hydrologic parameters from the TRMM to monitor evolving weather systems and natural hazard in real time. Ocean–atmosphere fluxes of

momentum, heat, and water will be produced at later stages. Seaflux is at website http://airsea-www.jpl.nasa.gov/seaflux.

7. Future

QuikSCAT was launched to reduce the data gap caused by the unexpected early demise of the Japanese spacecraft Midori (ADEOS-1). As originally planned, NSCAT was launched on ADEOS-1 in 1996, to be followed by two scatterometers, on ADEOS-2 and ADEOS-3, to provide more than a decade of ocean surface wind vectors. At present, another SeaWinds is planned on ADEOS-2, scheduled for launch in 2001. QuikSCAT will fly in tandem with ADEOS-2; they will be in complementary orbits to optimize the coverage by the scatterometers. The two SeaWinds are expected to demonstrate the importance of high wavenumber and high frequency forcing of the ocean. NASA is planning to supply an improved scatterrometer to GCOM (ADEOS-3), paving the way for an operational scatterometer system. The scatterometer will have strong scientific synergism with the ocean dynamic topography measured by Topex/Poseidon and JASON; with hydrologic parameters from TRMM and Advanced Microwave Scanning Radiometer (AMSR) on ADEOS-2 and Earth Observing System (EOS); and with ocean color by the Sea-Viewing Wide-Field-of-View Sensor (SeaWifs), the Moderate-Resolution Imaging Spectroradiometer (MODIS) on EOS, and Global Imager (GLI) on ADEOS-2.

The Ming emperor might have missed the opportunity to sustain the strength provided by superior naval technology. But, Chinese scientists of the 21th century should not let the wind of space technology pass them by. Vanguard technology feeds scientific innovation and leadership. If Chinese scientists will venture beyond well established methodologies and operational data to use a new generation of spacebased research sensors, they will put themselves not only in the forefront of environmental and climate research, but in a position to provide direction and thrust for the budding space program in China.

Acknowledgments

This study was performed at the Jet Propulsion Laboratory, California Institute of Technology, under contract with the National Aeronautics and Space Administration (NASA). It was jointly supported by the NSCAT, TRMM, the Physical Oceanography Program of NASA, and the Joint NOAA-NASA Program of Extended Data for Climate Changes. Son Nghiem kindly provided the computation of flood index. David Long generously made available spatially enhanced backscatter data over land and ice.

References

Atlas, R., S.C. Bloom, R.N. Hoffman, E. Brin, J. Ardizzone, J. Terry, D. Bungato, and J.C. Jusem, 1999: Geophysical validation of NSCAT winds using atmospheric data and analyses. *J. Geophys. Res., 104*, 11,405-11,424.

Chang, C.P., S. C. Lin, C. S. Liou, and W. T. Liu, 1999: An experiment using NSCAT winds in the numerical prediction of tropical mesoscale rainfall systems under the influence of terrain. *Geophys. Res. Lett., 26*, 311-314.

Graf, J., C. Sasaki, C. Winn, W.T. Liu, W. Tsai, M. Freilich, and D. Long, 1998: NASA Scatterometer Experiment. Asta Astronautica, 43, 397-407.

Hsu, C.S. and W.T. Liu, 1996: Wind and pressure fields near Tropical Cyclone Oliver derived from scatterometer observations. *J. Geophys. Res.*, *101*, 17,021-17,027.

Liu, W.T., H. Hu, and S.Yueh, 2000: QuikSCAT and Tropical Rain Measuring Mission reveal the interplay between dynamic and hydrologic parameters in Hurricane Floyd. EOS Trans. of AGU, in press.

Liu, W.T., W. Tang, and R. Atlas, 1996: Responses of the tropical Pacific to wind forcing as observed by spaceborne sensors and simulated by model. *J. Geophys. Res.*, 101, 16,345-16,359

Liu, W.T., W. Tang, and R. S. Dunbar, 1997: NASA Scatterometer Observes the Extratropical Transition of Pacific Typhoon. *Eos, Trans. of Amer. Geophys. Soc.*, *78*, 237 & 240.

Liu, W.T., W. Tang, and P.S. Polito, 1998: NASA Scatterometer provides global ocean-surface wind fields with more structures than numerical weather prediction. *Geophys. Res. Lett.*,*25*, 761-764

Liu, W.T., and X. Xie, 1999: Spacebased observations of the oceanic responses to seasonal changes of south Asian monsoons. *Geophys. Res. Lett.*, 126, 1473-1476

Long, D.G., and M.R. Drinkwater, 1999: Cryosphere Applications of NSCAT data. IEEE Trans Geos. Remote Sensing. 37, 1671-1684.

Nghiem, S.V., W.T. Liu, and X. Xie, 1999: Polarization reversal over flooded regions and applications to large-scale flood mapping with spaceborne scatterometers. *Proc. IGARSS'99*, IEEE.

Tang, W., and W.T. Liu, 1996: *Objective Interpolation of Scatterometer Winds.* JPL Publication 96-19, Jet Propulsion Laboratory, Pasadena, 16 pp.

List of Figures

Fig. 1 Over the ocean, white streamlines indicating wind direction are superimposed on the color image of wind speed at 0Z for 6 August 1999, derived from objective interpolation. Typical average backscatter coefficients over land and Antarctica are also added. The data are all based on observations by SeaWinds on QuikSCAT.

Fig. 2 Typhoon Olga is revealed by wind vectors (red arrows) from SeaWinds and surface precipitation (color image) from TRMM Microwave Imager on 31 July 1999, along the ground-tracks of QuikSCAT and TRMM, which are approximately three hours apart.

Fig. 3 Three-day average vector winds over ocean and flood indexes over land derived from SeaWinds on QuikSCAT observations, for four months in 1999. Topographic map for areas over 50-m elevation is plotted over flood indexes.

Fig. 4 Winter (December, January, and February) composites of anomalous cold events (La Niña). Dark arrows representing wind anomalies from SSMI are superimposed on color images of the anomalies of sea surface temperatures from AVHRR (upper), sea level changes from Topex/Poseidon (center), and precipitable water from SSMI (lower).

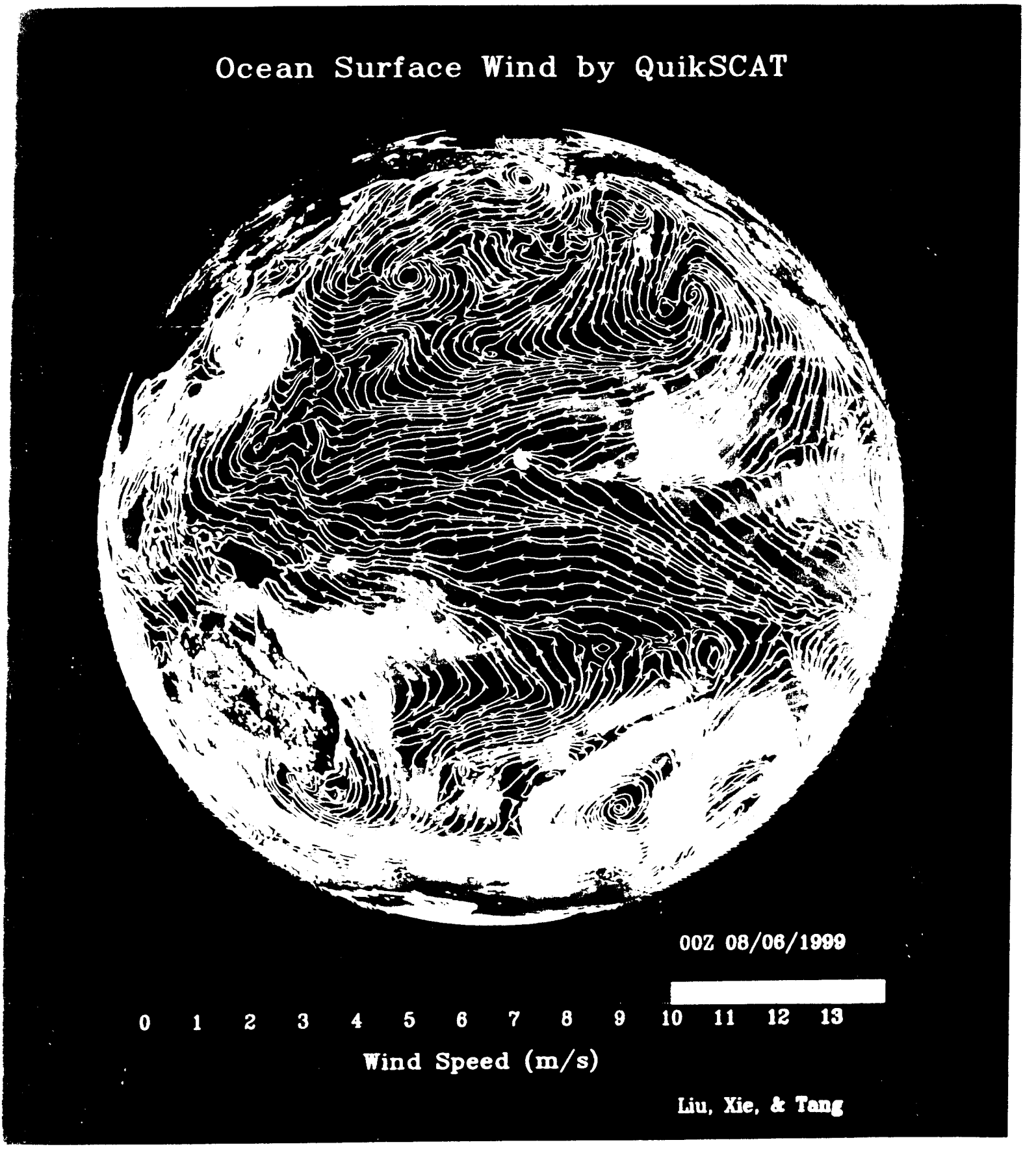
Ocean Surface Wind by QuikSCAT
00Z 08/06/1999
0 1 2 3 4 5 6 7 8 9 10 11 12 13
Wind Speed (m/s)
Liu, Xie, & Tang

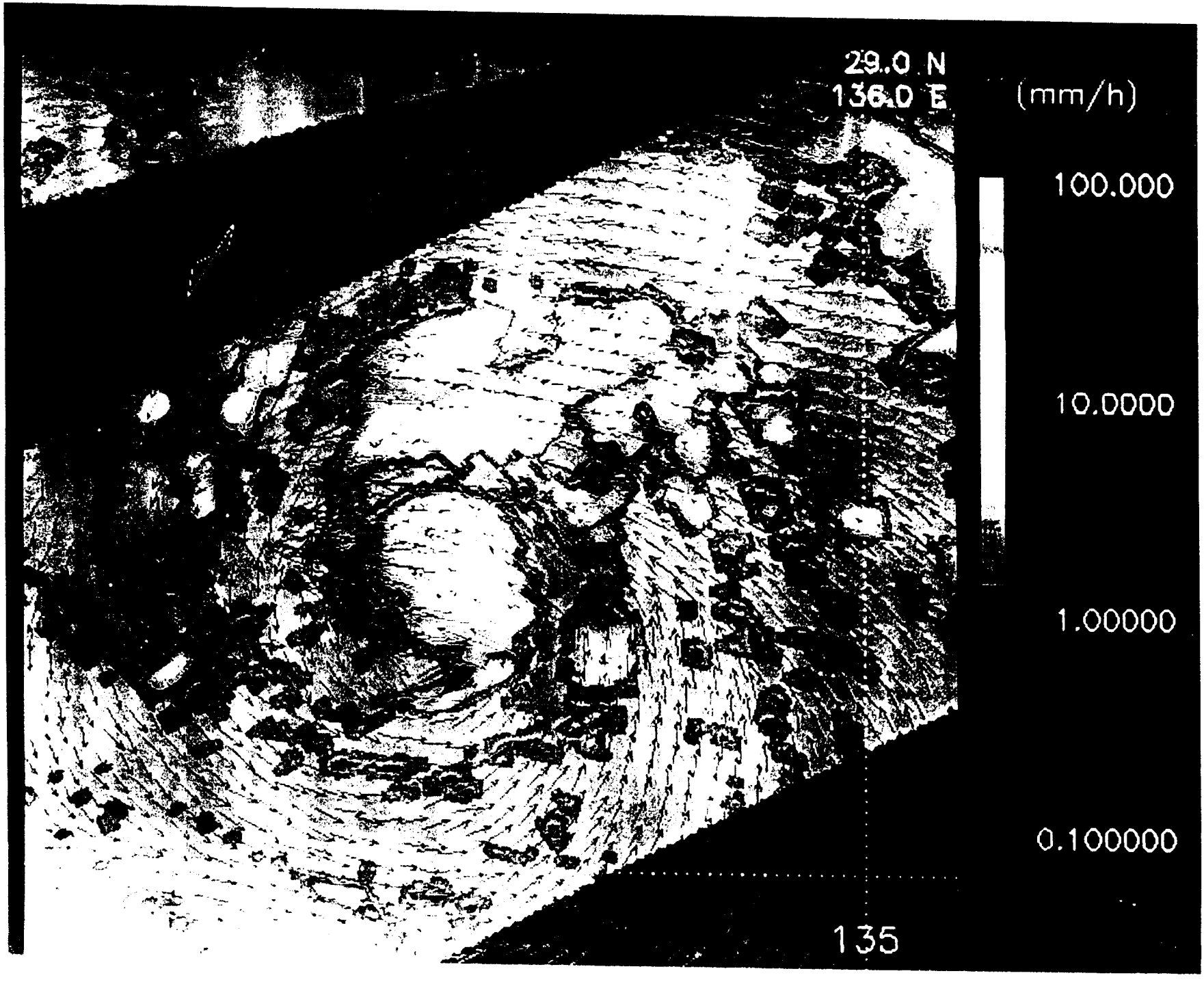
29.0 N
136.0 E
(mm/h)
100.000
10.0000
1.00000
0.100000
135

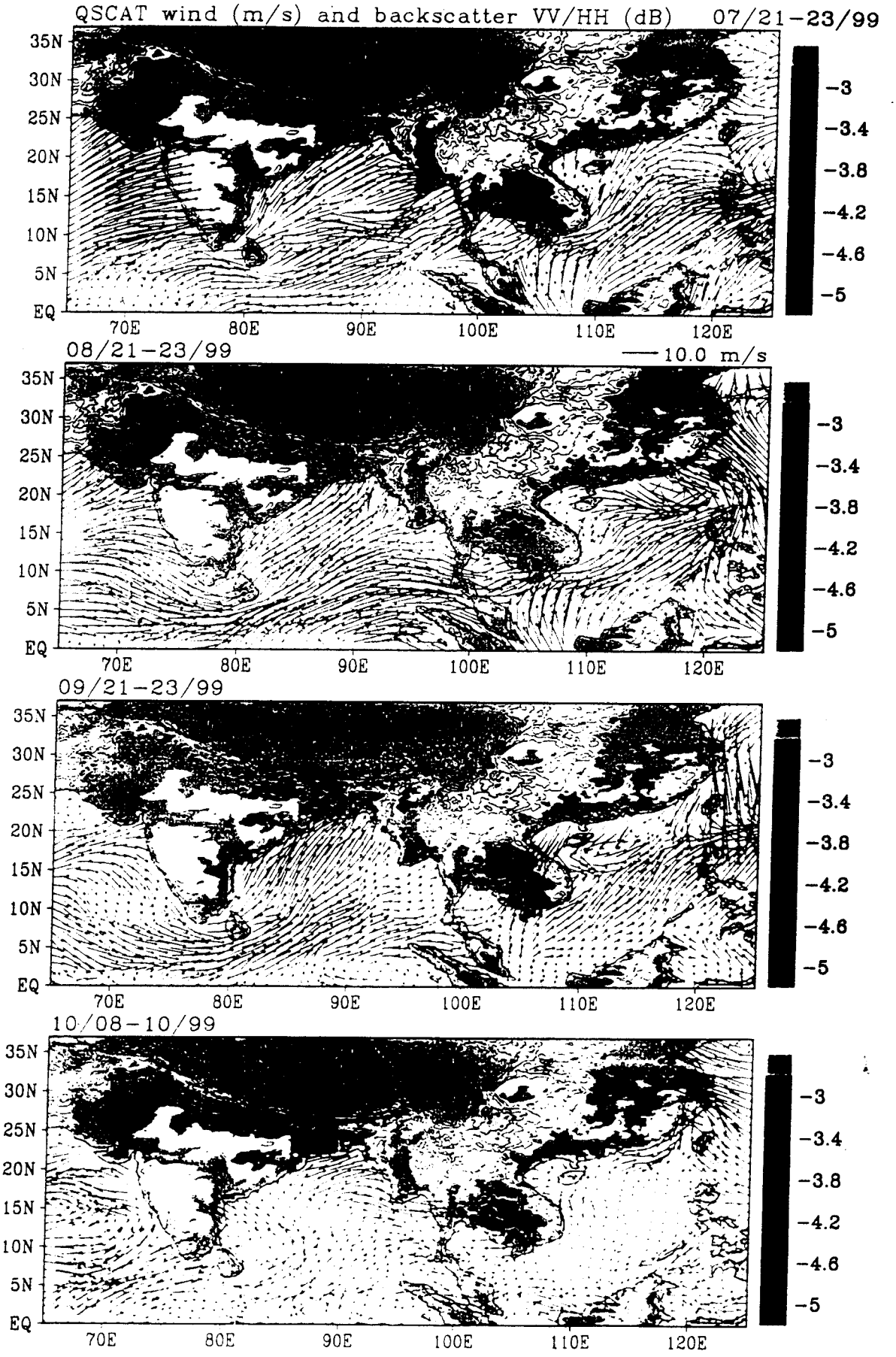
QSCAT wind (m/s) and backscatter VV/HH (dB) 07/21-23/99
35N
30N
25N
20N
15N
10N
5N
EQ
70E
80E
90E
100E
110E
120E
-3
-3.4
-3.8
-4.2
-4.6
-5
08/21-23/99
10.0 m/s
09/21-23/99
10/08-10/99

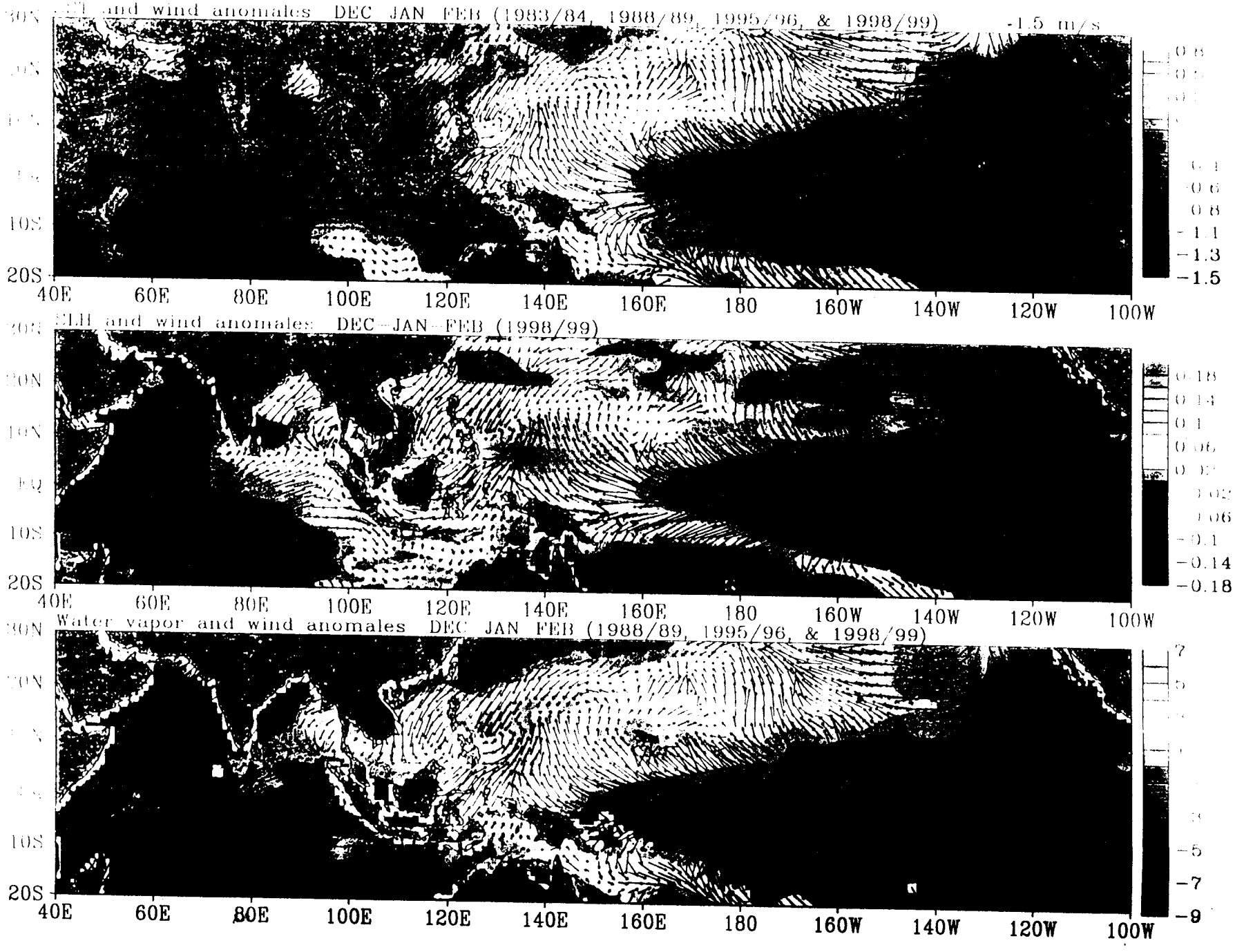
and wind anomales DEC JAN FEB (1983/84, 1988/89, 1995/96, & 1998/99)
-1.5 m/s
0.8
0.6
0.4
0.2
-0.2
-0.4
-0.6
-0.8
-1.1
-1.3
-1.5
10S
20S
40E
60E
80E
100E
120E
140E
160E
180
160W
140W
120W
100W
and wind anomales DEC-JAN-FEB (1998/99)
0.18
0.14
0.1
0.06
0.02
-0.02
-0.06
-0.1
-0.14
-0.18
10N
EQ
10S
20S
Water vapor and wind anomales DEC JAN FEB (1988/89, 1995/96, & 1998/99)
7
5
3
1
-1
-3
-5
-7
-9
10N
10S
20S